

Inert Higgs Dark Matter for CDF-II W -boson Mass and Detection Prospects

Yi-Zhong Fan,^{1,2} Tian-Peng Tang,^{1,2} Yue-Lin Sming Tsai,^{1,2} and Lei Wu³

¹Key Laboratory of Dark Matter and Space Astronomy,

Purple Mountain Observatory, Chinese Academy of Sciences, Nanjing 210033, China

²School of Astronomy and Space Science, University of Science and Technology of China, Hefei, Anhui 230026, China

³Department of Physics and Institute of Theoretical Physics,
Nanjing Normal University, Nanjing, 210023, China

(Dated: August 26, 2022)

The W -boson mass, which was recently measured at FermiLab with an unprecedented precision, suggests the presence of new multiplets beyond the Standard Model (SM). One of the minimal extensions of the SM is to introduce an additional scalar doublet in which the non-SM scalars can enhance W -boson mass via the loop corrections. On the other hand, with a proper discrete symmetry, the lightest new scalar in the doublet can be stable and play the role of a dark matter particle. We show that the inert two Higgs doublet model can naturally handle the new W -boson mass without violating other constraints and that the preferred dark matter mass is between 54 and 74 GeV. We identify three feasible parameter regions for the thermal relic density: the SA coannihilation, the Higgs resonance, and the $SS \rightarrow WW^*$ annihilation. We find that the first region can be fully tested by the High Luminosity Large Hadron Collider, the second region will be tightly constrained by direct detection experiments, and the third region could yield detectable GeV γ -ray and antiproton signals in the Galaxy that may have been observed by Fermi Large Area Telescope and the Alpha Magnetic Spectrometer AMS-02 experiment.

I. INTRODUCTION

The origin of mass is one of the most fundamental problems in modern physics. The central idea of generating masses of the electroweak gauge bosons in the standard model (SM) is the spontaneous symmetry breaking (SSB). Therefore, the precision measurement of the gauge boson masses is of great importance in testing the SSB mechanism. With the full dataset, the Collider Detector at Fermilab (CDF) collaboration has recently reported their newly measured W -boson mass $m_{W,\text{CDF-II}} = 80.4335 \pm 0.0094 \text{ GeV}$ [1], which deviates from the SM prediction $m_{W,\text{SM}} = 80.357 \pm 0.006 \text{ GeV}$ [2] about 7σ . This new measurement, characterized by its unprecedented precision, slightly conflicts with some previous measurements [3–6]. If confirmed in the future, as assumed in this Letter, the CDF II W -boson mass excess would strongly indicate the presence of new physics related with the SSB, such as models with extended Higgs sectors.

On the other hand, the existence of dark matter (DM) has been favored by various astrophysical and cosmological observations. For decades, Weakly Interacting Massive Particles (WIMPs) are considered as the strongest candidate for DM. One of the minimal scalar WIMP dark matter models is the inert two Higgs doublet model (i2HDM) [7–10], where one doublet H_1 is the SM Higgs doublet and the other doublet H_2 is hidden in the dark sector, given by

$$H_1 = \begin{pmatrix} G^+ \\ \frac{1}{\sqrt{2}}(v + h + iG^0) \end{pmatrix}, \quad H_2 = \begin{pmatrix} H^+ \\ \frac{1}{\sqrt{2}}(S + iA) \end{pmatrix}.$$

Here, G^\pm and G^0 are the charged and neutral Goldstone bosons, and $v \approx 246 \text{ GeV}$ is the vacuum expectation

value of the SM Higgs field. The discrete \mathbb{Z}_2 symmetry ($H_1 \rightarrow H_1$ and $H_2 \rightarrow -H_2$) is introduced to ensure the lightest scalar stable and cannot be spontaneously broken, i.e., $\langle H_2 \rangle = 0$. After the SSB, there will be five physical mass eigenstates, including two CP -even Higgs bosons h and S , one CP -odd Higgs boson A , and a pair of charged Higgs H^\pm . The \mathbb{Z}_2 -even scalar h is identified as the SM Higgs boson, and \mathbb{Z}_2 -odd scalar S or A can be the DM particle. Throughout this Letter, we assume that S is lighter and hence the DM particle. Because of the symmetry of exchanging S and A , the results will be unchanged for A being the DM [13–23].

In the i2HDM, the origin of the W -boson mass is still the Higgs mechanism, though due to contributions from the new Higgs bosons and interactions. Our model predicts deviations from the SM W -boson mass that can match that measured by CDF II. The corrections of the non-SM Higgs bosons to the squared W -boson mass can be expressed in term of the oblique parameters \mathcal{S} , \mathcal{T} , and \mathcal{U} [11, 12], i.e.,

$$\Delta m_W^2 = \frac{\alpha c_W^2 m_Z^2}{c_W^2 - s_W^2} \left[-\frac{\mathcal{S}}{2} + c_W^2 \mathcal{T} + \frac{c_W^2 - s_W^2}{4s_W^2} \mathcal{U} \right], \quad (1)$$

where c_W and s_W are cosine and sine of Weinberg angle. The fine structure constant and Z boson mass are denoted as α and m_Z . In Eq. (1), the dominant contribution to the W -boson mass arises from \mathcal{T} parameter, which is sensitive to the mass splitting of new particles running in the loop of gauge boson self-energy. Meanwhile, when the charged Higgs bosons are lighter than the neutral Higgs bosons, they produce a positive \mathcal{S} and thus reduce the corrections to W -boson mass. Therefore, a heavy H^\pm but light S and A are preferred to enhance the value of Δm_W^2 . Indeed, we will show that the i2HDM with $m_S/m_{H^\pm} < 0.5$ and $m_A/m_{H^\pm} < 1$ can naturally

account for the W -boson mass anomaly and offer a successful thermal WIMP paradigm without violating other constraints. The upcoming collider and DM experiments will be able to effectively probe the favored regions.

II. METHODOLOGY

The scalar potential of i2HDM can be written as

$$V = \mu_1^2 |H_1|^2 + \mu_2^2 |H_2|^2 + \lambda_1 |H_1|^4 + \lambda_2 |H_2|^4 + \lambda_3 |H_1|^2 |H_2|^2 + \lambda_4 |H_1^\dagger H_2|^2 + \frac{\lambda_5}{2} \left\{ (H_1^\dagger H_2)^2 + \text{h.c.} \right\}. \quad (2)$$

Taking $m_h = 125$ GeV and $v = 246$ GeV, there are six free parameters in the scalar potential after the electroweak symmetry breaking, namely μ_2^2 , λ_2 , λ_3 , λ_4 and λ_5 . Note that λ_2 is a phenomenologically invisible interaction at the tree-level, which is only involved in the four-points interaction of \mathbb{Z}_2 -odd scalar bosons. The relationships between the other four parameters and the physical masses are given by

$$\begin{aligned} m_h^2 &= -2\mu_1^2 = 2\lambda_1 v^2, \\ m_S^2 &= \mu_2^2 + \frac{1}{2}(\lambda_3 + \lambda_4 + \lambda_5)v^2 = \mu_2^2 + \lambda_S v^2, \\ m_A^2 &= \mu_2^2 + \frac{1}{2}(\lambda_3 + \lambda_4 - \lambda_5)v^2 = \mu_2^2 + \lambda_A v^2, \\ m_{H^\pm}^2 &= \mu_2^2 + \frac{1}{2}\lambda_3 v^2, \end{aligned} \quad (3)$$

where λ_S and λ_A represent the hSS and hAA couplings, respectively. For convenience, we use the mass splitting parameters $\Delta^0 = m_A - m_S$ and $\Delta^\pm = m_{H^\pm} - m_S$ to study the new contributions to the W -boson mass and DM relic density in the i2HDM. In the following investigation, we choose the input parameters as $\{m_S, \Delta^0, \Delta^\pm, \lambda_2, \lambda_5\}$.

We explore the parameter space of i2HDM with the Markov chain Monte Carlo method in the ranges of

$$\begin{aligned} 30.0 &\leq m_S / \text{GeV} \leq 4000.0, \\ 10^{-4} &\leq \Delta^0 / \text{GeV} \leq 500.0, \\ 1.0 &\leq \Delta^\pm / \text{GeV} \leq 500.0, \\ -1.0 &\leq \lambda_S \leq 1.0, \\ 10^{-10} &\leq \lambda_2 \leq 4.2. \end{aligned} \quad (4)$$

We calculate the mass spectrum, theoretical bounds on the Higgs potential, and electroweak precision observables with 2HDMC [12]. Since the observed DM relic density and DM direct detection provide the stringent constraints, we compute the DM observables such as the relic density, the annihilation cross section, and the spin-independent DM-nucleon scattering cross section with micrOMEGAs [24]. We also consider the collider constraints from the null results of searching for new scalar bosons, exotic Higgs decays, mono-X searches, and Higgs decay to diphoton $R_{\gamma\gamma}$ as in Ref. [18].

Likelihood type	Constraints
Step	perturbativity, stability, unitarity [12]
Step	LEP-II [25], OPAL [26]
Half-Gaussian	PandaX-4T [27]
Half-Gaussian	exotic Higgs decays [28]
Gaussian	relic abundance [29]
Gaussian	$R_{\gamma\gamma}$ [30]
Gaussian	EWPT [2] or $m_{W,\text{CDF-II}}$ [1]

TABLE I. Likelihood distributions and constraints used in our analysis.

In order to present the allowed parameter space, we use “*Profile Likelihood*” method [31] to get rid of nuisance parameters while showing the two dimensional contours. In Table I, we list the above experimental constraints incorporated in our likelihood functions. The total χ_{tot}^2 is to sum over the individual χ^2 of these constraints. We use Gaussian likelihood with

$$\chi^2 = \left(\frac{\mu - \mu_{\text{exp}}}{\sigma} \right)^2 \quad \text{and} \quad \sigma = \sqrt{\sigma_{\text{theo}}^2 + \sigma_{\text{exp}}^2}, \quad (5)$$

where μ is the theoretical prediction and μ_{exp} is the experimental central value. The uncertainty σ includes both theoretical and experimental errors. For those Half-Gaussian functions, we can set $\mu_{\text{exp}} = 0$ based on the null signal. We use the hard cuts for the theoretical bounds, Large Electron-Positron collider (LEP-II), and Omni-Purpose Apparatus at LEP (OPAL) limits.

To examine the impact of the new CDF II m_W measurement, we perform two sets of numerical scans by taking two different likelihoods for electroweak precision data. Please bear in mind that these two scans share the same constraints in Table I, except for electroweak precision likelihood. The first likelihood, which is denoted as PDG2020 and does not take into account the latest CDF-II m_W data, includes the previous complete electroweak precision measurements that are parameterized by three oblique parameters $\mathcal{S} = -0.01 \pm 0.1$, $\mathcal{T} = 0.03 \pm 0.12$ and $\mathcal{U} = 0.02 \pm 0.11$ (all intervals are for 68% confidence level). The correlation coefficients of $(\mathcal{S}, \mathcal{T})$, $(\mathcal{S}, \mathcal{U})$ and $(\mathcal{T}, \mathcal{U})$ are 0.92, -0.8 , and -0.93 , respectively [2]. We refer the readers to Ref. [18] for the implementation of the covariance matrix with oblique parameters. For the second, we use the CDF II W -boson mass measurement $m_{W,\text{CDF-II}} = 80.4335 \pm 0.009$ GeV as the electroweak precision test likelihood function.

On the other hand, since the DM indirect detection constraints likely suffer from some systematic uncertainties, we will not include them in the likelihood but compare our allowed parameter space with the limits set by the Fermi Large Area Telescope observations of dwarf Spheroidal galaxies [32] as well as the signal regions of the Fermi Large Area Telescope Galactic Center γ -ray excess [33–36], and the Alpha Magnetic Spectrometer AMS-02 experiment antiproton excess [37–40].

We adopt the Markov chain Monte Carlo scans by using the code EMCEE [41]. To reach a good coverage of the parameter space, we perform several scans and finally collect $\mathcal{O}(4.5 \times 10^6)$ data points. The confidence intervals are calculated from the tabulated values of $\Delta\chi^2 \equiv -2\ln(\mathcal{L}/\mathcal{L}_{\max})$. For a two-dimensional plot, the 95% confidence (2σ) region is defined by $\Delta\chi^2 \leq 5.99$ under the assumption of approximate Gaussian likelihood.

III. NUMERICAL RESULTS AND DISCUSSIONS

As mentioned above, we present two sets of results based on the likelihoods summarized in Table I. One is in gray (see Fig.1 and 2), which is obtained from the global fit with PDG2020 electroweak precision test (EWPT) [2]. While the other, marked in green, blue and red, takes into account the new CDF II m_W data in the fit [1].

In Fig. 1, we display the 95% allowed regions on the planes of m_S/m_{H^\pm} versus m_W as well as m_A/m_{H^\pm} versus m_W with and without constraint of the latest CDF II m_W measurement. The color regions present the favored dominant DM production mechanisms in the early Universe, including the SA co-annihilation (green), the Higgs resonance (blue), and $SS \rightarrow WW^*$ annihilation (red). We find that the loop correction to m_W is dominated by the oblique parameter T so that a large mass splitting between the charged Higgs bosons and neutral Higgs bosons can enhance W -boson mass sizably. Besides, we note that the mass ratios of m_S/m_{H^\pm} and m_A/m_{H^\pm} have to be less than one, i.e., $m_S/m_{H^\pm} < 0.5$ and $0.35 < m_A/m_{H^\pm} < 1$, since they can produce a negative oblique parameter S to further increase the W -boson mass. There is a clear gap at $m_W \sim 80.4$ GeV between gray and other three colors in both $(m_S/m_{H^\pm}, m_W)$ and $(m_A/m_{H^\pm}, m_W)$ planes, owing to the fact that the central value of m_W from PDG2020 differs with the recent CDF II measurement by 7σ . Hence, they do not overlap in m_W -axis at the 95% significance level.

In Fig. 2, we present the allowed 95% regions for above two cases on the planes of m_S versus m_A as well as m_S versus m_{H^\pm} . It can be seen that the DM mass m_S is bounded within the range of 54 – 74 GeV. The previous higher mass region of $m_S > 500$ GeV for $S - A - H^\pm$ co-annihilation is excluded. To account for the new CDF II W -boson mass, the mass differences between the charged Higgs bosons and neutral Higgs bosons should be enhanced; hence the mass degeneracy needed by the $S - A - H^\pm$ co-annihilation is broken. The explicit correlations between the oblique parameters and new mass spectra can be found in Supplemental Material, where the relevant multileptons plus missing energy signature [42–44] are also discussed. Therefore, only three different favored parameter space for the DM relic density remains: SA coannihilation with $m_S \approx m_A$ (green region), the Higgs resonance with $m_S \approx m_h/2$ (blue region), and the off-shell annihilation of $SS \rightarrow WW^*$

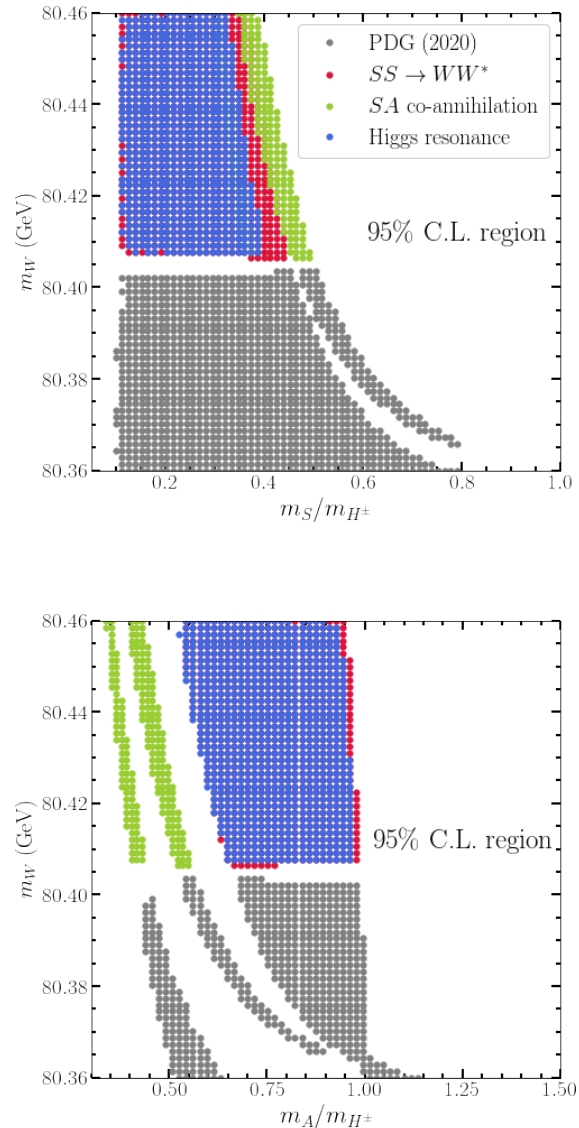


FIG. 1. The 95% confidence level allowed regions for three DM production mechanisms: SA coannihilation (green), the Higgs resonance (blue), and $SS \rightarrow WW^*$ annihilation (red) on the plane of m_S/m_{H^\pm} versus m_W , and m_A/m_{H^\pm} versus m_W . The gray regions are allowed by the data of PDG2020 but excluded by $m_{W,\text{CDF-II}}$. The 95% region of m_S/m_{H^\pm} has been narrowed down to ≤ 0.5 .

(red region). The first two mechanisms are in general with small couplings but the four-point interaction $\propto \lambda_3 = 2(m_{H^\pm}^2 - \mu_2^2)/v^2$ can efficiently govern DM annihilation for $m_S > 60$ GeV even though one of W -bosons is off-shell. One can see that a kink of the coannihilation region, induced by the four-point interaction, appears at $m_S \sim 60$ GeV in Fig. 2.

In Fig. 3, we show the prospects of testing the above three favored scenarios in future collider and dark mat-

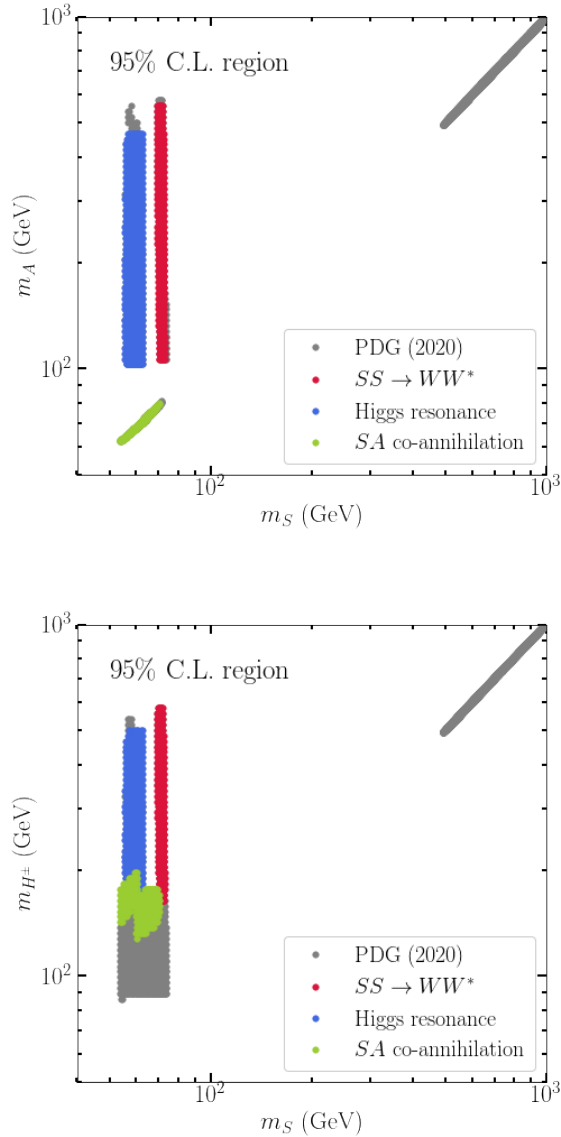


FIG. 2. Same as Fig. 1, but on the planes of m_S versus m_A , and m_S versus m_{H^\pm} . Note that the low m_{H^\pm} region (i.e., ≤ 120 GeV) as well as the high m_S region (i.e., ≥ 74 GeV), despite of viable for the data of PDG2020, have been ruled out by $m_{W,\text{CDF-II}}$.

ter experiments. In the case of the Higgs resonance, we find that the DM-Higgs coupling is within the range of $|\lambda_S| < 0.003$. The survived region covers the range of $4 \times 10^{-50} \text{ cm}^2 \leq \sigma_p^{SI} \leq 5 \times 10^{-47} \text{ cm}^2$, which has been tightly constrained by the latest PandaX-4T limit. Most of the remaining parameter space will be probed by the DM direct detection experiments in the near future. In contrary, a large portion of the survived parameter space of SA coannihilation and $SS \rightarrow WW^*$ regions is below the so-called neutrino floor and hence beyond the scope of the conventional DM direct detec-

tion experiments. Fortunately, these two scenarios can be probed in future collider and DM indirect detection experiments. To be specific, due to a small mass splitting between S and A (see middle panel), we recast the current exclusion limit from the LHC search for the compressed supersymmetry [47], and also show the expected bound for the integrated luminosity 750 fb^{-1} . We can see that the SA coannihilation region can be fully covered at the future LHC. In addition, we note that the DM annihilation cross section can be around the thermal cross-section $\langle \sigma v \rangle \sim 10^{-26} \text{ cm}^3 \text{ s}^{-1}$ in SA coannihilation, Higgs resonance and $SS \rightarrow WW^*$ regions. For the first two cases, the DM mass m_S has to be in the range of $61 \text{ GeV} < m_S < 64 \text{ GeV}$. On the other hand, the DM mass in $SS \rightarrow WW^*$ case lies in the range of $69 \text{ GeV} < m_S < 73 \text{ GeV}$. Interestingly, such mass ranges coincide with the dark matter mass needed to account for the Galactic Center excess and Alpha Magnetic Spectrometer AMS-02 antiproton excess [48]. Therefore, if all these intriguing anomalies are further confirmed, the i2HDM would be a natural model to accommodate them.

IV. CONCLUSION

The Collider Detector at Fermilab collaboration has just reported their latest measurement of m_W with unprecedented accuracy, whose value is above the standard model prediction at a significance level of 7σ . Such a W -boson mass anomaly, if confirmed by other experiments in the future, would point toward the presence of new physics that can be related to dark matter. The simplest dark matter model to account for the anomaly is the i2HDM. After addressing current theoretical and astrophysical constraints, we obtain viable regions of $m_S/m_{H^\pm} < 0.5$ and $0.35 < m_A/m_{H^\pm} < 1$, for which the mass degeneracy of coannihilation at $m_S > 500$ GeV has been broken. This is remarkably different from the pre-2022 data. As a result, the heavy dark matter mass region has been thoroughly excluded and the charged Higgs must be heavier than S and A . The DM mass is inferred to be between 54 GeV and 74 GeV and the thermal relic density was governed by the process of either the Higgs resonance, or SA coannihilation, or $SS \rightarrow WW^*$ annihilation. The $m_{W,\text{CDF-II}}$ favored dark matter mass range is well consistent with being a weakly interacting massive particle or WIMP, which is the most extensively discussed dark matter candidate. Encouragingly, the GeV γ -ray excess in the Galactic center and the possible GeV antiproton excess do consistently suggest a dark matter particle within the same mass range. Further dedicated efforts are highly needed to explore whether these two astrophysical signals and the $m_{W,\text{CDF-II}}$ indeed have the common origin. Finally, it should be mentioned that, though the above conclusions are drawn with $m_{W,\text{CDF-II}}$, the adaption of the latest full electroweak precision data [49] yields rather similar results, as shown in the Supplemental Material.

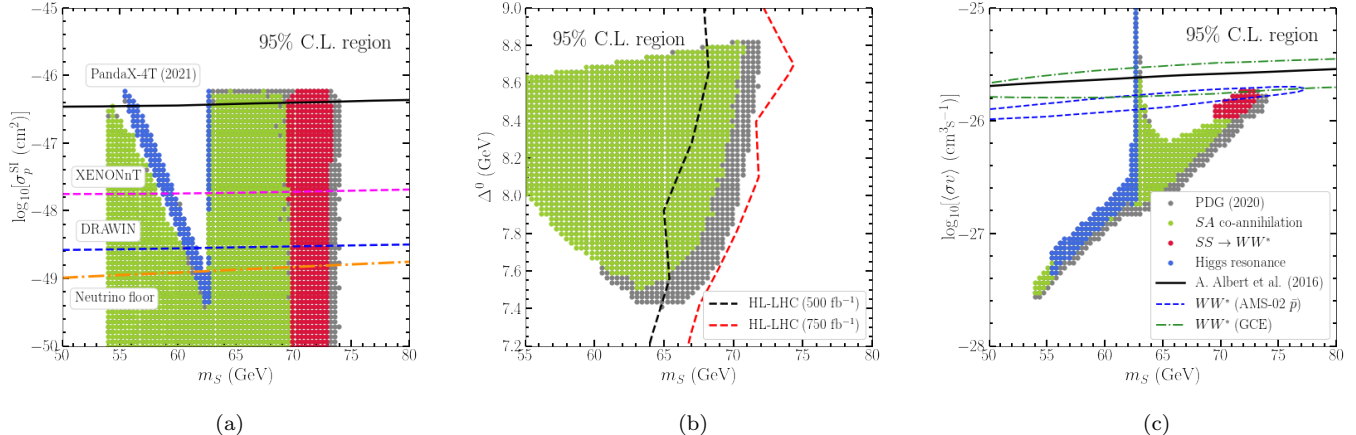


FIG. 3. The 95% favored regions of σ_p^{SI} [panel (a)], Δ^0 [panel (b)], and $\langle\sigma v\rangle$ [panel (c)] as a function of dark matter mass (i.e., m_S). The Higgs resonance region and the SA coannihilation region can be efficiently probed by the ongoing dark matter direct detection experiments [45, 46] and the High Luminosity Large Hadron Collider [47], respectively. The $SS \rightarrow WW^*$ parameter region as well as a small fraction of the first and second regions are in agreement with that needed to reproduce the GeV γ -ray excess in the Galactic center and/or the GeV antiproton anomaly (the 2σ constraint counters are adopted from [48]).

ACKNOWLEDGMENTS

We appreciate Andrew Fowlie for his kind and helpful discussions. This work was supported in part by the National Natural Science Foundation of China (No. 11921003 and No. U1738210) and by the Key Research Program of the Chinese Academy of Sciences (No. XDPB15).

SUPPLEMENTAL MATERIAL

Appendix A: Additional information on the distribution of the physical parameters

Here we present more complete information on the distribution of the physical parameters constrained by current experimental/astrophysical constraints.

In Fig. 4, we show the DM-Higgs coupling as a function of m_S . The PLANCK relic density constraint results in a small favored region because other regions are corresponding to DM relic abundance $\Omega_\chi h^2$ overproduced. Because of the correlation $\Omega_\chi h^2 \propto 1/\langle\sigma v\rangle$, a tiny coupling requires specific mechanisms, such as the SA coannihilation (green), the Higgs resonance (blue) and $SS \rightarrow WW^*$ annihilation via four points interaction (red), to boost the annihilation cross section. The PDG2020 data has already imposed stringent constraints on λ_S and the inclusion of $m_{W,\text{CDF}}$ has just narrowed down the viable region slightly.

Since Δm_W^2 is proportional to $-\mathcal{S}$, \mathcal{T} and \mathcal{U} [see Eq. (1) in the main text], the sizeable W -boson mass anomaly thus calls for a negative \mathcal{S} or almost zero if positive and a relative large \mathcal{T} . Note that in i2HDM usually the ab-

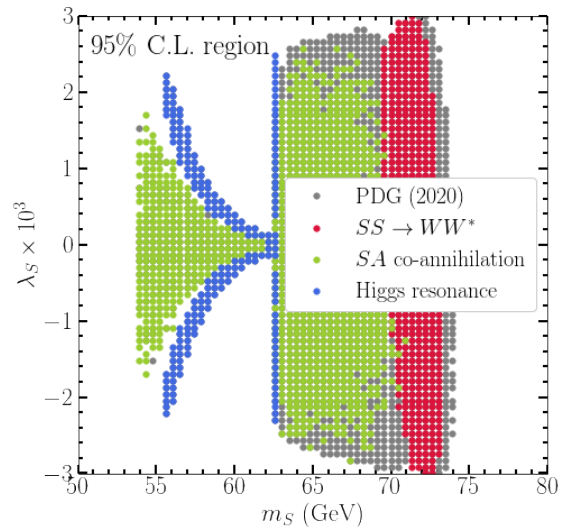


FIG. 4. The 95% C.L. allowed regions: SA coannihilation (green), the Higgs resonance (blue), and $SS \rightarrow WW^*$ annihilation (red) on the plane of m_S versus λ_S . The gray region is for the data of PDG2020. Clearly, λ_S is very small.

solute value of \mathcal{U} is smaller than that of \mathcal{T} by one or two orders. In particular, a positive \mathcal{S} , which is only allowed in the SA coannihilation scenario, would favor a high \mathcal{T} . The correlations between oblique parameters and mass spectra are displayed in Fig.5. As anticipated, $m_{W,\text{CDF-II}}$ sets stringent constraints on the ranges of \mathcal{S} and \mathcal{T} and we have $\mathcal{S} \leq 0.025$ and $\mathcal{T} \geq 0.07$.

In Fig. 6a and Fig. 6b, we present the Δ^0 and Δ^\pm as a

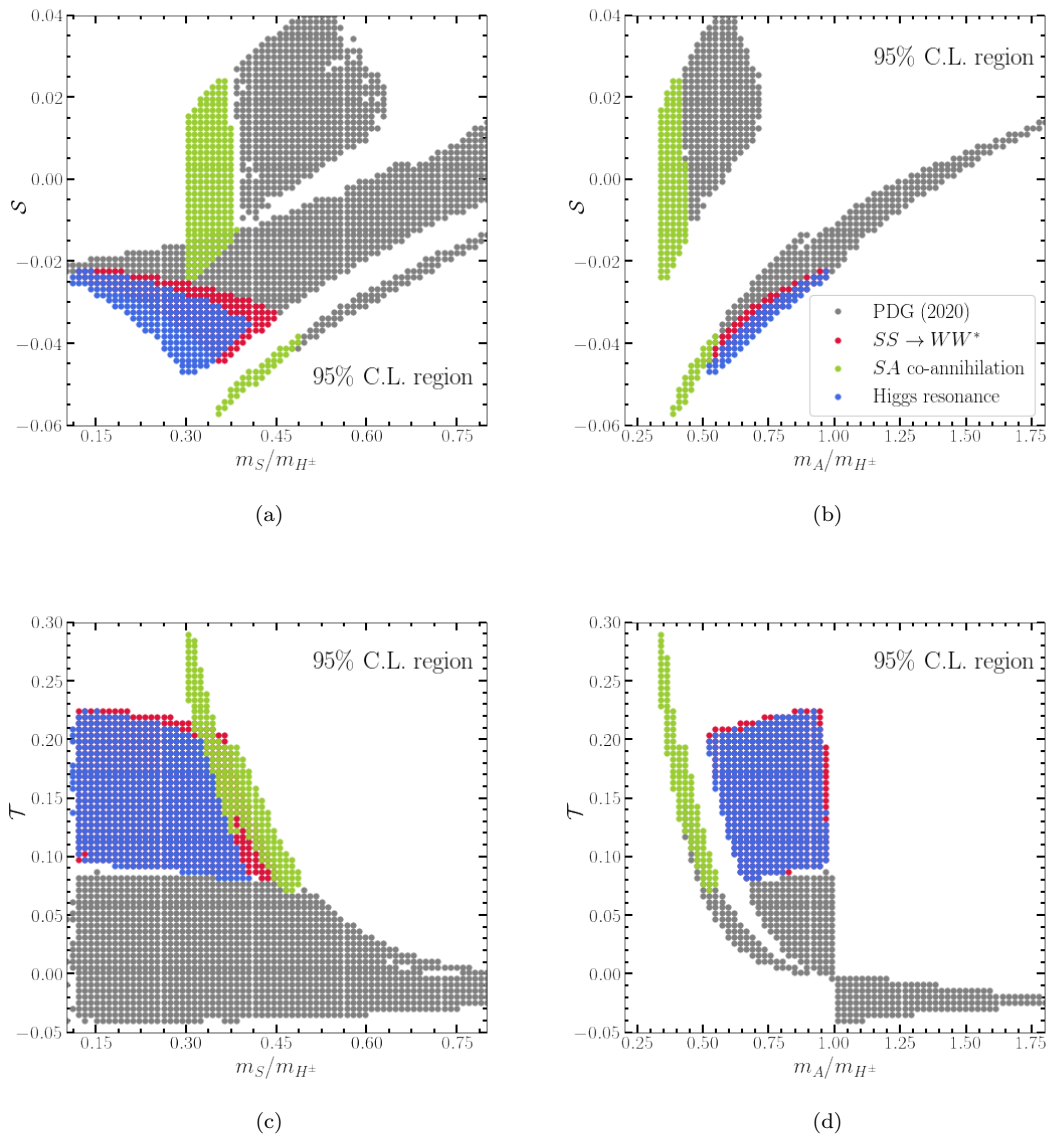


FIG. 5. The correlations between oblique parameters and mass spectra. The CDF II W -boson mass measurement plays a key role in shaping the viable ranges of S , \mathcal{T} and \mathcal{U} . To reproduce the data, S should be negative or almost zero if positive, while \mathcal{T} is relatively high.

function of m_S in a wide range of $40 \text{ GeV} < m_S < 4 \text{ TeV}$. In the absence of the CDF II W -boson mass measurement data, $m_S > 500 \text{ GeV}$ is allowed under the coannihilation condition $m_S \approx m_A \approx m_{H^\pm}$, as found in the literature [14, 19]. Such a massive DM region, however, has been convincingly excluded by $m_{W, \text{CDF-II}}$. For the SA coannihilation scenario, we have a Δ^0 clustering in the range of $7.5 - 8.8 \text{ GeV}$. The mass splitting $\Delta^0 \sim 30 - 520 \text{ GeV}$ is needed for the other two scenarios. The CDF II m_W anomaly also requires a $60 \text{ GeV} < \Delta^\pm < 530 \text{ GeV}$. Although a large Δ^\pm can enhance the coupling of H^\pm pair production as searched in the multi-leptons plus missing energy signature [42, 43], the heavy H^\pm makes

the cross section suppressed that the sensitivity can only reach $\Delta^\pm \sim 50 \text{ GeV}$ [44] at $m_S > 50 \text{ GeV}$.

Appendix B: Results with full electroweak precision data

Since the new m_W data from CDF II is slightly in tension with other electroweak precision measurements, it is interesting to check what happens with the combined analysis. In this subsection, we therefore present the results based on the likelihood which includes all the electroweak precision measurements as done in PDG2020.

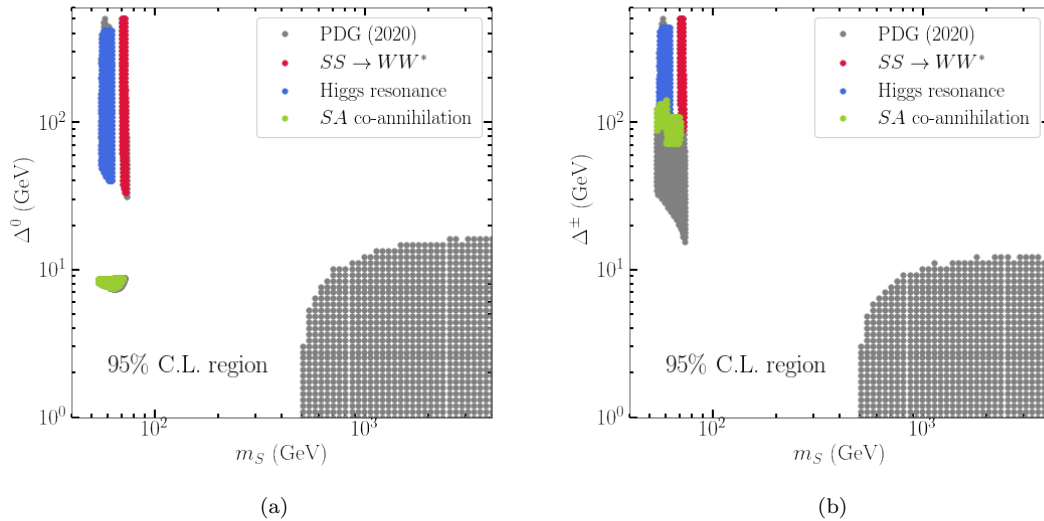


FIG. 6. The favored 95% regions of Δ^0 [panel (a)] and Δ^\pm [panel (b)] as a function of the dark matter mass (i.e., m_S). Different colors represent different physical processes governing the thermal relic density, as labeled in the plots. The regions of $m_S > 500$ GeV are also presented but they have been excluded by the CDF II m_W measurement.

For the full likelihood (EWPT2022), we adopt the new covariance matrix provided in Ref. [49] where the CDF II m_W data is included in their global fitting. The updated oblique parameter are $\mathcal{S} = 0.06 \pm 0.1$, $\mathcal{T} = 0.11 \pm 0.12$ and $\mathcal{U} = 0.14 \pm 0.09$, and the correlation coefficients of $(\mathcal{S}, \mathcal{T})$, $(\mathcal{S}, \mathcal{U})$ and $(\mathcal{T}, \mathcal{U})$ are 0.90, -0.59 , and -0.85 , respectively. We note that the full EWPT2022 likelihood sets slightly weaker constraints in comparison to that with the sole m_W data. In addition, EWPT2022 likelihood enlarges our global minimum χ^2 from 6.87 to

14.01.

In Fig. 7, we update the 2σ distributions shown in Fig.1 and Fig.2 with the constraints of EWPT2022. In comparison to Fig.1, now the 95% allowed regions of m_W have been (slightly) shifted downward and the gap between PDG2020 and CDF II results disappears. Anyhow, our other results and conclusions are essentially unchanged by comparing Fig.2 in the main text with Fig. 7c and 7d. The same holds for Fig.3 and for simplicity here we do not show the updated plots.

-
- [1] T. Aaltonen *et al.* [CDF], *Science* **376**, no.6589, 170-176 (2022) doi:10.1126/science.abk1781
- [2] P. A. Zyla *et al.* [Particle Data Group], *PTEP* **2020**, no.8, 083C01 (2020) doi:10.1093/ptep/ptaa104
- [3] S. Schael *et al.* [ALEPH, DELPHI, L3, OPAL and LEP Electroweak], *Phys. Rept.* **532** (2013), 119-244 doi:10.1016/j.physrep.2013.07.004
- [4] R. Aaij *et al.* [LHCb], *JHEP* **01** (2022), 036 doi:10.1007/JHEP01(2022)036
- [5] M. Aaboud *et al.* [ATLAS], *Eur. Phys. J. C* **78** (2018) no.2, 110 [erratum: *Eur. Phys. J. C* **78** (2018) no.11, 898] doi:10.1140/epjc/s10052-017-5475-4
- [6] V. M. Abazov *et al.* [D0], *Phys. Rev. Lett.* **108** (2012), 151804 doi:10.1103/PhysRevLett.108.151804
- [7] N. G. Deshpande and E. Ma, *Phys. Rev. D* **18**, 2574 (1978) doi:10.1103/PhysRevD.18.2574
- [8] E. Ma, *Phys. Rev. D* **73**, 077301 (2006) doi:10.1103/PhysRevD.73.077301 [arXiv:hep-ph/0601225 [hep-ph]].
- [9] R. Barbieri, L. J. Hall and V. S. Rychkov, *Phys. Rev. D* **74**, 015007 (2006) doi:10.1103/PhysRevD.74.015007 [arXiv:hep-ph/0603188 [hep-ph]].
- [10] L. Lopez Honorez, E. Nezri, J. F. Oliver and M. H. G. Tytgat, *JCAP* **02**, 028 (2007) doi:10.1088/1475-7516/2007/02/028 [arXiv:hep-ph/0612275 [hep-ph]].
- [11] M. E. Peskin and T. Takeuchi, *Phys. Rev. D* **46**, 381-409 (1992) doi:10.1103/PhysRevD.46.381
- [12] D. Eriksson, J. Rathsmann and O. Stal, *Comput. Phys. Commun.* **181**, 189-205 (2010) doi:10.1016/j.cpc.2009.09.011 [arXiv:0902.0851 [hep-ph]].
- [13] A. Arhrib, Y. L. S. Tsai, Q. Yuan and T. C. Yuan, *JCAP* **06**, 030 (2014) doi:10.1088/1475-7516/2014/06/030 [arXiv:1310.0358 [hep-ph]].
- [14] A. Goudelis, B. Herrmann and O. Stål, *JHEP* **09**, 106 (2013) doi:10.1007/JHEP09(2013)106 [arXiv:1303.3010 [hep-ph]].
- [15] A. Ilnicka, M. Krawczyk and T. Robens, *Phys. Rev. D* **93**, no.5, 055026 (2016) doi:10.1103/PhysRevD.93.055026 [arXiv:1508.01671 [hep-ph]].
- [16] M. A. Díaz, B. Koch and S. Urrutia-Quiroga, *Adv. High Energy Phys.* **2016**, 8278375 (2016)

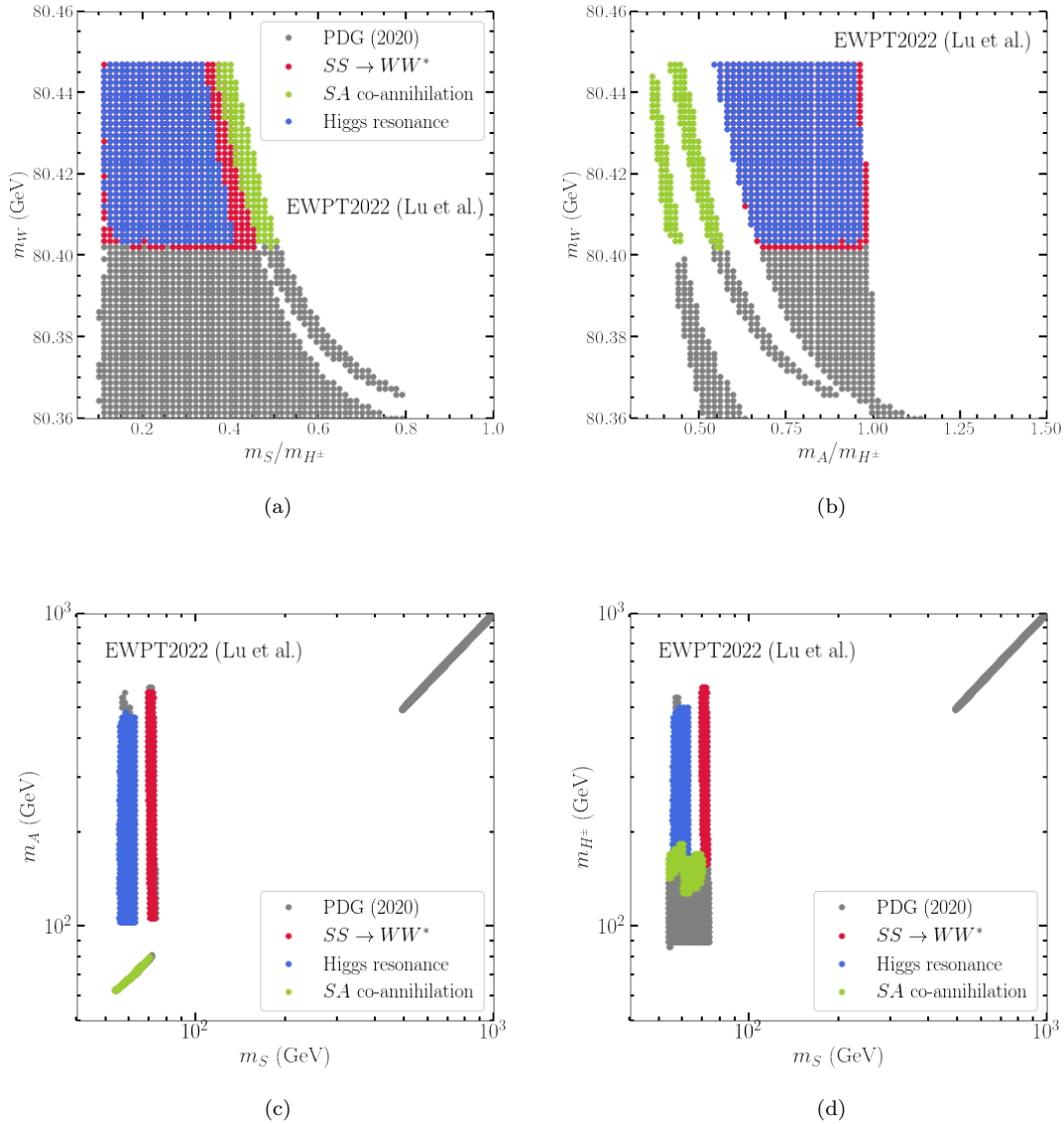


FIG. 7. The same as Fig. 1 and Fig. 2 in the main text but with the constraints of the new global EW fit [49].

- doi:10.1155/2016/8278375 [arXiv:1511.04429 [hep-ph]].
- [17] A. Belyaev, G. Cacciapaglia, I. P. Ivanov, F. Rojas-Abatte and M. Thomas, Phys. Rev. D **97**, no.3, 035011 (2018) doi:10.1103/PhysRevD.97.035011 [arXiv:1612.00511 [hep-ph]].
- [18] Y. L. S. Tsai, V. Tran and C. T. Lu, JHEP **06**, 033 (2020) doi:10.1007/JHEP06(2020)033 [arXiv:1912.08875 [hep-ph]].
- [19] E. M. Dolle and S. Su, Phys. Rev. D **80**, 055012 (2009) doi:10.1103/PhysRevD.80.055012 [arXiv:0906.1609 [hep-ph]].
- [20] S. Banerjee, F. Boudjema, N. Chakrabarty and H. Sun, Phys. Rev. D **104**, 075003 (2021) doi:10.1103/PhysRevD.104.075003 [arXiv:2101.02166 [hep-ph]].
- [21] S. Banerjee, F. Boudjema, N. Chakrabarty and H. Sun, Phys. Rev. D **104**, 075005 (2021) doi:10.1103/PhysRevD.104.075005 [arXiv:2101.02170 [hep-ph]].
- [22] L. Lopez Honorez and C. E. Yaguna, JCAP **01**, 002 (2011) doi:10.1088/1475-7516/2011/01/002 [arXiv:1011.1411 [hep-ph]].
- [23] S. Banerjee, F. Boudjema, N. Chakrabarty and H. Sun, Phys. Rev. D **104**, 075004 (2021) doi:10.1103/PhysRevD.104.075004 [arXiv:2101.02167 [hep-ph]].
- [24] G. Bélanger, F. Boudjema, A. Goudelis, A. Pukhov and B. Zaldivar, Comput. Phys. Commun. **231**, 173-186 (2018) doi:10.1016/j.cpc.2018.04.027 [arXiv:1801.03509 [hep-ph]].
- [25] K. A. Olive *et al.* [Particle Data Group], Chin. Phys. C **38**, 090001 (2014) doi:10.1088/1674-1137/38/9/090001

- [26] G. Abbiendi *et al.* [OPAL], Eur. Phys. J. C **32**, 453-473 (2004) doi:10.1140/epjc/s2003-01466-y [arXiv:hep-ex/0309014 [hep-ex]].
- [27] Y. Meng *et al.* [PandaX-4T], Phys. Rev. Lett. **127**, no.26, 261802 (2021) doi:10.1103/PhysRevLett.127.261802 [arXiv:2107.13438 [hep-ex]].
- [28] M. Aaboud *et al.* [ATLAS], Phys. Rev. Lett. **122**, no.23, 231801 (2019) doi:10.1103/PhysRevLett.122.231801 [arXiv:1904.05105 [hep-ex]].
- [29] N. Aghanim *et al.* [Planck], Astron. Astrophys. **641**, A6 (2020) [erratum: Astron. Astrophys. **652**, C4 (2021)] doi:10.1051/0004-6361/201833910 [arXiv:1807.06209 [astro-ph.CO]].
- [30] [ATLAS], ATLAS-CONF-2018-031.
- [31] W. A. Rolke, A. M. Lopez and J. Conrad, Nucl. Instrum. Meth. A **551**, 493-503 (2005) doi:10.1016/j.nima.2005.05.068 [arXiv:physics/0403059 [physics]].
- [32] A. Albert *et al.* [Fermi-LAT and DES], Astrophys. J. **834**, no.2, 110 (2017) doi:10.3847/1538-4357/834/2/110 [arXiv:1611.03184 [astro-ph.HE]].
- [33] D. Hooper and L. Goodenough, Phys. Lett. B **697**, 412-428 (2011) doi:10.1016/j.physletb.2011.02.029 [arXiv:1010.2752 [hep-ph]].
- [34] B. Zhou, Y. F. Liang, X. Huang, X. Li, Y. Z. Fan, L. Feng and J. Chang, Phys. Rev. D **91**, no.12, 123010 (2015) doi:10.1103/PhysRevD.91.123010 [arXiv:1406.6948 [astro-ph.HE]].
- [35] F. Calore, I. Cholis and C. Weniger, JCAP **03**, 038 (2015) doi:10.1088/1475-7516/2015/03/038 [arXiv:1409.0042 [astro-ph.CO]].
- [36] T. Daylan, D. P. Finkbeiner, D. Hooper, T. Linden, S. K. N. Portillo, N. L. Rodd and T. R. Slatyer, Phys. Dark Univ. **12**, 1-23 (2016) doi:10.1016/j.dark.2015.12.005 [arXiv:1402.6703 [astro-ph.HE]].
- [37] M. Y. Cui, Q. Yuan, Y. L. S. Tsai and Y. Z. Fan, Phys. Rev. Lett. **118**, no.19, 191101 (2017) doi:10.1103/PhysRevLett.118.191101 [arXiv:1610.03840 [astro-ph.HE]].
- [38] A. Cuoco, M. Krämer and M. Korsmeier, Phys. Rev. Lett. **118**, no.19, 191102 (2017) doi:10.1103/PhysRevLett.118.191102 [arXiv:1610.03071 [astro-ph.HE]].
- [39] M. Y. Cui, X. Pan, Q. Yuan, Y. Z. Fan and H. S. Zong, JCAP **06**, 024 (2018) doi:10.1088/1475-7516/2018/06/024 [arXiv:1803.02163 [astro-ph.HE]].
- [40] I. Cholis, T. Linden and D. Hooper, Phys. Rev. D **99**, no.10, 103026 (2019) doi:10.1103/PhysRevD.99.103026 [arXiv:1903.02549 [astro-ph.HE]].
- [41] D. Foreman-Mackey, D. W. Hogg, D. Lang and J. Goodman, Publ. Astron. Soc. Pac. **125**, 306-312 (2013) doi:10.1086/670067 [arXiv:1202.3665 [astro-ph.IM]].
- [42] G. Belanger, B. Dumont, A. Goudelis, B. Herrmann, S. Kraml and D. Sengupta, Phys. Rev. D **91**, no.11, 115011 (2015) doi:10.1103/PhysRevD.91.115011 [arXiv:1503.07367 [hep-ph]].
- [43] G. Aad *et al.* [ATLAS], Eur. Phys. J. C **80**, no.2, 123 (2020) doi:10.1140/epjc/s10052-019-7594-6 [arXiv:1908.08215 [hep-ex]].
- [44] A. Belyaev, U. Blumenschein, A. Freegard, S. Moretti and D. Sengupta, [arXiv:2204.06411 [hep-ph]].
- [45] E. Aprile *et al.* [XENON], JCAP **11**, 031 (2020) doi:10.1088/1475-7516/2020/11/031 [arXiv:2007.08796 [physics.ins-det]].
- [46] M. Schumann, L. Baudis, L. Büttikofer, A. Kish and M. Selvi, JCAP **10**, 016 (2015) doi:10.1088/1475-7516/2015/10/016 [arXiv:1506.08309 [physics.ins-det]].
- [47] G. Aad *et al.* [ATLAS], Phys. Rev. D **101**, no.5, 052005 (2020) doi:10.1103/PhysRevD.101.052005 [arXiv:1911.12606 [hep-ex]].
- [48] C. R. Zhu, M. Y. Cui, Z. Q. Xia, Z. H. Yu, X. Huang, Q. Yuan and Y. Z. Fan, [arXiv:2204.03767 [astro-ph.HE]].
- [49] C. T. Lu, L. Wu, Y. Wu and B. Zhu, [arXiv:2204.03796 [hep-ph]].